Bragg waveguide grating as a 1D photonic band gap structure: COST 268 modelling task

J. ČTYROKÝ[1*], S. HELFERT[2], R. PREGLA[2], P. BIENSTMAN[3],
R. BAETS[3], R. DE RIDDER[4], R. STOFFER[4], G. KLAASSE[4],
J. PETRÁČEK[5], P. LALANNE[6], J.-P. HUGONIN[6]
AND R.M. DE LA RUE[7]

[1]*Institute of Radio Engineering and Electronics, Chaberská 57, 182 51 Praha 8, Czech Republic;*
[2]*FernUniversität, Allgemeine und Theoretische Elektrotechnik, D-58084 Hagen, Germany;*
[3]*Ghent University, Department of Information Technology/IMEC, Sint-Pietersnieuwstraat 41, B-9000
Ghent, Belgium;*
[4]*University of Twente, MESA Research Institute, P.O. Box 217, 7500 AE Enschede, The Netherlands;*
[5]*Institute of Physical Engineering, Brno University of Technology, Technická 2, 616 69 Brno, Czech
Republic;*
[6]*Institut d'Optique Théorique et Appliquée/CNRS, BP 147, 91403 Orsay Cedex, France;*
[7]*Optoelectronics Research Group, Department of Electronics and Electrical Engineering, The University,
Glasgow, G12 8QQ, Scotland, UK*
*(*author for correspondence: E-mail: ctyroky@ure.cas.cz)*

Abstract. Modal reflection, transmission and loss of deeply etched Bragg waveguide gratings were modelled by six European laboratories using independently developed two-dimensional (2D) numerical codes based on four different methods, with very good mutual agreement. It was found that (rather weak) material dispersion of the SiO_2/Si_3N_4 system does not significantly affect the results. The existence of lossless Floquet–Bloch modes in deeply etched gratings was confirmed. Based on reliable numerical results, the physical origin of out-of-plane losses of 1D or 2D photonic band gap structures in slab waveguides is briefly discussed.

Key words: optical waveguide modelling, photonic band gap structure, photonic crystal, waveguide grating

1. Introduction

Photonic crystals (PC) and photonic band gap structures (PBG) are very promising building blocks of novel photonic components and devices representing the highest level of innovation in light generation, routing, and switching (Yablonovich 1987; Joannopoulos *et al.* 1995; Mekis *et al.* 1996). As the fully three-dimensional (3D) PCs working in the optical domain are still difficult to fabricate, two-dimensional (2D) PCs formed in a dielectric slab ('membrane') or in a slab waveguide represent an attractive alternative (Benisty *et al.* 1997) (Johnson *et al.* 1999). In these structures, light propagation is governed by diffractive effects in the two dimensions of the 2D photonic crystal, and by the classical 'refractive guiding' in the third (usually vertical) dimension.

It is known that 2D PCs in slab waveguides support lossless propagation of eigenmodes (Johnson *et al.* 1999) (Bloch or Floquet modes) if the refractive index contrast is large enough, and the existence of separate band gaps for guided modes of TE and TM polarisations has been proven both theoretically and experimentally (Benisty *et al.* 1997; Johnson *et al.* 1999). However, for technical applications, PCs of finite size are to be used, and their connection to the 'outer world' by classical refractive waveguides is of practical interest. Working Group 2 of the European Action COST 268 'Wavelength-scale photonic components for telecommunications' possesses a forum for interested researchers from several European labs to discuss these problems. Within this forum, a modelling task has been formulated that represents a simplified version of the problem, namely to calculate spectral properties of a deeply etched short Bragg grating in a comparatively high-contrast optical waveguide. The waveguide material structure was chosen to match closely with published work (Charlton *et al.* 1997) and with the expectation that test structures with this structure and the parameters modelled will be fabricated and measured.

This task evolved from the recent modelling exercise formulated within COST 240 (Guekos 1998), the predecessor of COST 268. Although the problem is closely related to a simpler problem of a 1D PC, the task is essentially 2D, deals with a PC of a finite size, and accurately tackles the important problem of out-of-plane losses in a vertically asymmetric slab PBG structure.

Originally, the exercise was aimed at the comparison of modelling approaches and verification of computer codes used by different participating laboratories. Soon after an initial period, several independent methods based on very different principles (modal, finite-difference time–domain (FDTD), and grating methods) have been found to possess essentially identical results, and are thus believed to be very reliable. It opened the possibility of accurate 2D numerical modelling of radiation losses of the slab PCs in more depth.

2. Definition of the modelling task

The present version of the modelling task was specified in June 2000 and posted on the web at the URL http://www.ure.cas.cz/dpt130/cost268/. Its aim is to calculate the spectral dependence of the (modal) power transmittance $T(\lambda)$, reflectance $R(\lambda)$ and loss $L(\lambda) = 1 - T(\lambda) - R(\lambda)$ of the fundamental TE mode in the waveguide Bragg grating with 20 rectangular grooves in a relatively broad spectral range from 0.8 to 1.6 μm. The waveguide is schematically depicted in Fig. 1.

The waveguide is formed by a Si_3N_4 layer of the thickness $d_g = 500$ nm deposited onto a SiO_2 substrate, with air as a superstrate. The refractive
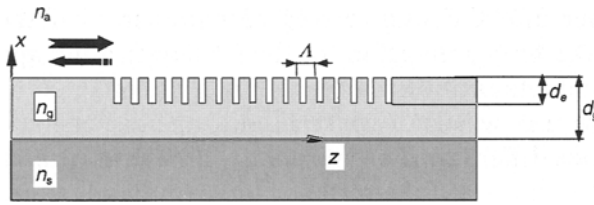
Fig. 1. Bragg grating in a planar waveguide.

index n_s of the substrate is given by the dispersion formula for silicon dioxide fabricated by the MCVD method,

$$n_s^2 = b_0 + \frac{b_1}{\lambda^2 + b_2} + \frac{b_3}{\lambda^2 + b_4}, \tag{1}$$

with the coefficients $b_0 = 2.979864$, $b_1 = 8.777808 \times 10^{-3}$, $b_2 = 1.0609 \times 10^{-2}$, $b_3 = 84.06224$, $b_4 = -96.0$, λ is the wavelength in µm. The dispersion formula for the Si_3N_4 guiding layer is

$$n_g^2 = a^2 + \frac{b\lambda^2}{\lambda^2 - c^2}, \tag{2}$$

where $a = 1.147, b = 2.578, c = 0.1472$. It was derived from measured data at the University of Twente. The refractive index of the superstrate (air) is 1.00. The spectral dependence of the refractive indices of the substrate and the guiding layer is plotted in Fig. 2.

The grating period was originally fixed to be 430 nm, the widths of the 'tooth' and the 'groove' were chosen equal, i.e., 215 nm ('mark–space ratio' is 1:1). The groove etching depth d_e varies from 0 to 750 nm in steps of 125 nm. (Groove depths greater than 500 nm mean that the groove is etched through
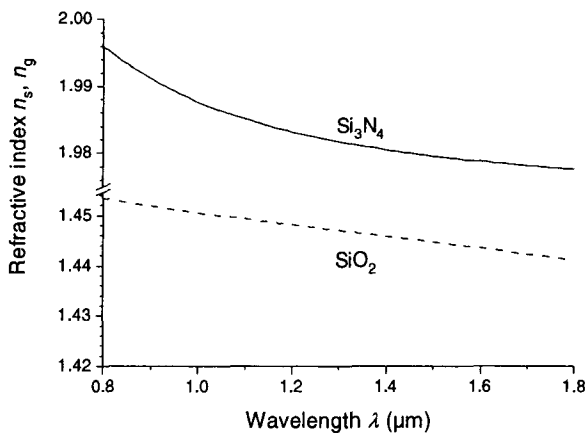

Fig. 2. Wavelength dependence of the refractive indices of the substrate and the guiding layer.

the guiding layer into the substrate.) The parameters of the grating were chosen so that the Bragg reflection for the shallow grating appeared close to the optical telecommunication wavelength of 1.55 µm.

The modelling task was later generalised to the dispersionless case and to mark–space ratios different from unity, as will be briefly discussed below.

3. Modelling methods and laboratories participating in the comparison

Within the framework of the COST 268 Working Group 2, six laboratories participated in the modelling task with six independently developed computer codes based on four different modelling methods. Their overview is shown in Table 1.

In the method of lines (MoL) the fields are discretised in the cross-section, and the derivatives with respect to the cross-section coordinates are approximated by finite differences (FDs) (Pregla 1995). Combining the FD into an operator matrix and by computing the eigenvalues and eigenvectors of this matrix, the eigenmodes are determined. To model radiation, absorbing boundary conditions are introduced into the FD-scheme. Since there exist many papers dealing with this algorithm, (see, e.g. Scarmozzino *et al.* 2000) and the references herein) only a few remarks concerning the implementation are given here. To avoid the use of exponentially increasing terms, which lead to numerical problems in the case of long sections, an admittance transformation concept was developed (Rogge and Pregla 1993; Pregla 1999). To model the grating the algorithm described in (Helfert and Pregla 1998) was used, where the admittance transformation was combined with the Floquet theorem leading to a very fast algorithm, even for a very high number of periods.

The eigenmode expansion method BEP1 was implemented at Ghent University in the CAMFR modelling framework (Bienstman and Baets

Table 1. Modelling methods and participating laboratories

Method	Laboratory	References
MoL	Allg u. Theor. Elektrotechnik, FernUniversität Hagen, D	(Helfert and Pregla 1998)
BEP1	Dept. of Information Technology/ IMEC, Ghent University, B	(Bienstman and Baets 2001)
BEP2	Inst. of Radio Engineering and Electronics, Prague, CZ	(Sztefka and Nolting 1993; Čtyroký *et al.* 1998)
BEP3	Dept. of Physical Engineering, Brno University of Technology, CZ	(Sztefka and Nolting 1993)
GT	Institut d'Optique Théorique et Appliquée/CNRS, F	(Silberstein *et al.* 2001)
FDTD	MESA Research Institute, University of Twente, NL	(Taflove 1995; Stoffer *et al.* 2000)

2001). It can handle both slab waveguide geometries and circular symmetric structures. The boundary conditions are based on the complex coordinate formulation (Chew *et al.* 1999) of perfectly matched layers (Bérenger 1994). The local eigenmodes of each layer are found in the complex plane by the so-called root-tracking method (Bienstman *et al.* 2001). First, the propagation constants are located for the structure without any PML. These modes lie on the coordinate axes, where they are readily found. Subsequently, the absorption in the PML is gradually increased to the desired value, and the propagation constants are tracked as they move into the complex plane. To calculate the scattering matrices of the entire finite periodic grating, the numerically stable S-matrix scheme is used, in combination with a recursive technique that makes the calculation time logarithmic in the number of periods (Bienstman and Baets 2001).

The bi-directional mode expansion and propagation method BEP2 used by the IREE Prague is conceptually very similar to that developed at Ghent University. It is based on the original paper (Sztefka and Nolting 1993) and has been described in detail in (Čtyroký *et al.* 1998). The boundary conditions in the form of the perfectly matched layers (Bérenger 1994) using the formulation of complex coordinate stretching (Chew *et al.* 1999) have been implemented. Complex propagation constants of the eigenmodes of each waveguide section are calculated using the transfer matrix method. Zeros of the dispersion function in the complex plane are localised by the method similar to the root-tracking method (Bienstman and Baets 2001), too. The fact that the dispersion function is a regular function of the complex propagation constant (squared) is efficiently utilised in the application of the Newton method in the complex plane. The calculation of the modal reflectance, transmittance, and modal losses makes use of the Floquet–Bloch (FB) modes of the grating structure defined as eigenmodes of the transfer matrix of one period of the grating (Čtyroký *et al.* 1998). The corresponding eigenvalues determine the relative phase shift of the Bloch modes after one period of propagation. Using the FB modes makes the computation time essentially independent of the number of grating periods and improves the numerical stability of the method. Numerical stability of the algorithm is attained by the application of the immitance method (Sudbø 1994) in the FB formalism.

The BEP3 code developed independently at the Brno University of Technology is essentially similar to the BEP1 and BEP2 methods described above, except that longitudinal propagation along the grating is calculated in terms of the eigenmodes of the corresponding waveguide sections, without transition to the basis of FB eigenmodes.

The method described by (Silberstein *et al.* 2001) used at the Institut d'Optique Théorique et Appliquée (IOTA) is inspired by grating theory (GT) and belongs to the general class of frequency–domain modal methods. In every longitudinally uniform section of the waveguide, the modes are com-

puted as eigenvectors. The computation relies on analytical Fourier expansions of the permittivity and of the electromagnetic fields. Perfectly matched layers are used to bound the computational domain.

The FDTD method is a very general and well-known method for calculating electromagnetic field distributions in structures of arbitrary geometry, based on a direct discretisation of Maxwell's equations. The UT-implementation is based on Yee's mesh and absorbing boundary conditions of the PML type have been applied. A very detailed and practical overview of the FDTD method is given in the book by (Taflove 1995). In order to obtain the spectral characteristics using FDTD, a very short ($\sim$1 fs) pulse, having sufficiently broad frequency content, is launched into the slab waveguide. Its time evolution is calculated and transmission and reflection spectra are obtained by Fourier transforming the resulting time series at appropriate locations in the structure. Since transmission and reflection coefficients for the guided fundamental slab mode are sought, it is necessary to take the overlap integral of the local modal field with the field distribution calculated using FDTD. This is complicated due to the broad spectral range and the frequency dependence of the modal field distribution. A similar complication arises in launching a proper modal pulse. However, these complications are more than outweighed by the fact that the FDTD method offers a unique chance to compare results obtained by spectral–modal methods with those of the time–domain method.

4. Results of the modelling task

4.1. INFLUENCE OF MATERIAL DISPERSION

Material dispersion was introduced into the calculations with the aim of making the anticipated comparison with experimental data more realistic. However, it significantly hampers the application of the FDTD method. To estimate the error introduced by neglecting material dispersion we calculated the results using one of the BEP methods (BEP2), both when including material dispersion and when keeping the refractive indices of the substrate and the guiding layer constant, corresponding to the wavelength of 1.55 μm, namely $n_s = 1.44409$, $n_g = 1.97916$. For brevity, the results for only three grating etching depths are presented in Fig. 3.

From the comparison of results in Fig. 3 it clearly (and rather surprisingly) follows that material dispersion of the material system SiO_2/Si_3N_4 has only a very small effect on the spectral curves of modal reflectance and transmittance of the waveguide Bragg grating, the spectral interval of which spans more than one octave, even though the characters of the material dispersion
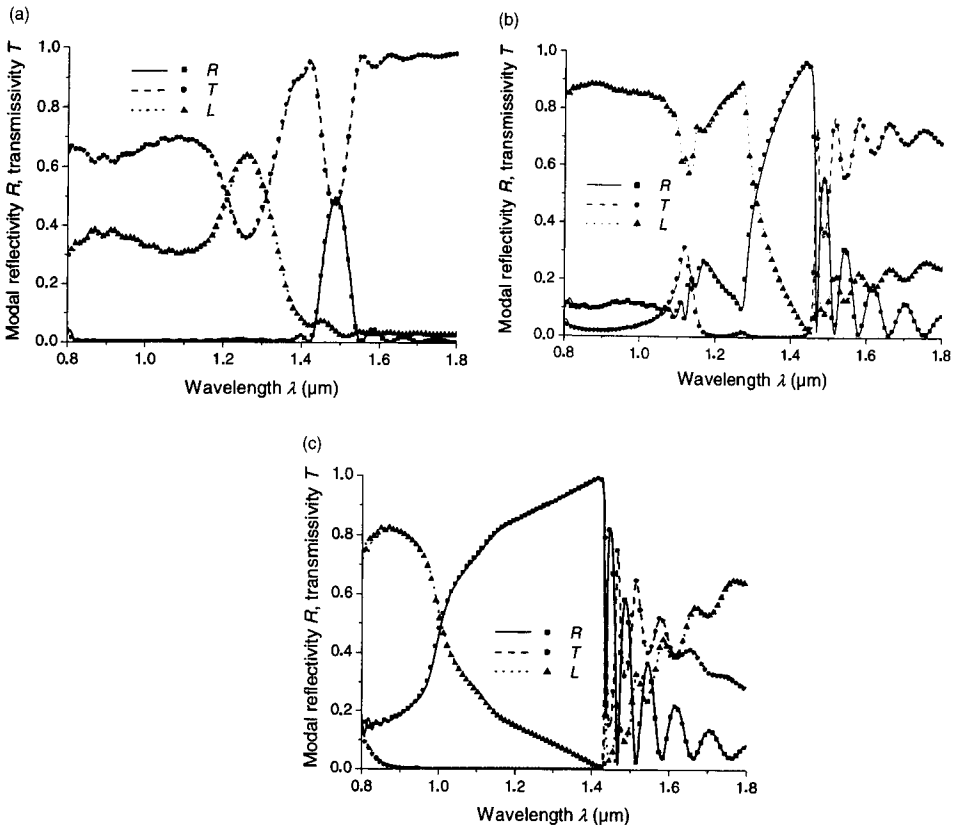
Fig. 3. The influence of material dispersion on the spectral dependence of the modal reflectance R, transmittance T and loss ($L = 1 - R - T$) of the waveguide Bragg grating. Groove depths: (a) 125 nm, (b) 375 nm, (c) 625 nm. Curves – with dispersion; solid curve – reflectance, dashed – transmittance. Points – without dispersion, circle – reflectance, triangle – transmittance.

of the substrate and the guiding layer are rather different, as follows from Fig. 2. The influence of the material dispersion manifests itself by a small spectral shift that is observable only in regions where the curves exhibit sharp changes or oscillations due to interference effects, especially in the long-wavelength ('dielectric') side of the band gap. One can thus expect that the predictions of the 'dispersionless' FDTD method might be used for the comparison with experimental data just as well as the results of modal methods in which the material dispersion is fully taken into account.

4.2. COMPARISON OF RESULTS OBTAINED BY DIFFERENT METHODS

The spectral dependences of the modal transmission, reflection, and losses of the same gratings as in Fig. 3 were calculated using four modal methods (the
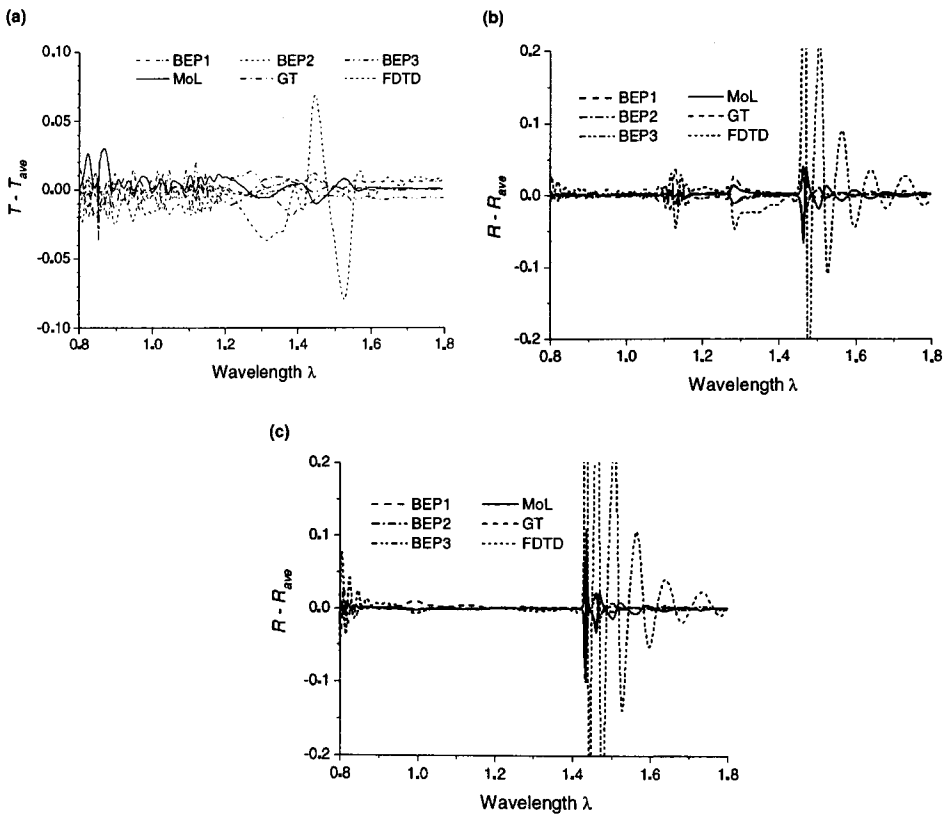
(a)

(b)

(c)

Fig. 4. Comparison of spectral dependencies of the modal reflectance R or transmittance T of Bragg waveguide gratings calculated by six modelling methods. (a) Transmittance, etching depth 125 nm, (b) reflectance, 375 nm, (c) reflectance, 625 nm.

MoL and all three BEPs), the grating technique method GT, and the FDTD method. The graphs in Fig. 4 represent differences between the transmittances (a) and reflectances (b, c) calculated by the individual methods and the averaged results of the methods MoL, BEP1, BEP2, BEP3, and GT. These methods work in the spectral region and are thus naturally able to take into account the dispersion. The differences among the results of different methods are thus much more clearly visualised.

It can easily be concluded from the graphs that all methods possess very similar results that typically differ only by a few percent. Larger deviations are observed only in spectral regions where the curves exhibit abrupt changes or periodic oscillations. For deeply etched gratings, (Fig. 4(b), (c)) deviations occur mainly in the region close to the long-wavelength band gap edge. Closer inspection reveals that the differences are in most cases due to very small spectral shifts between the curves. Quite naturally, the FDTD method is the most susceptible to such spectral shift because it neglects dispersion. It

Table 2. Important characteristics of the modelling methods

Method	Hardware/software	Number of modes/ steps in x/z	RAM memory (MB)	Computing time (s)	Equiv. time @ 1 GHz (s)
MoL	Pentium II 333 MHz, Matlab	150/2	5	11500	3830
BEP1	Pentium III 933 MHz, C++	70/2	10	432	403
BEP2	Athlon 1.33 GHz, Fortran 90/95	70/2	5	684	910
BEP3	Athlon 500 MHz, C++	70/2	2	12000	6000
GT	PC 600 MHz, Matlab	70/2	2	4550	2730
FDTD	Athlon 600 MHz, C++	250/1250	21	7200	4320

is very probable that the difference between the FDTD and other methods could be strongly suppressed by a small change of the refractive indices used for the calculation. All important features of the spectral curves are nevertheless well reproduced, both qualitatively and quantitatively, by all methods, including the FDTD. The results can thus be considered a reliable and successful cross-check of the correctness of the algorithms.

It is interesting to compare characteristic features of the modelling methods that are important for their application in modelling PC structures in more detail. For this comparison we selected (rather randomly) the grating with the etch depth of 625 nm (see Fig. 3(c)). In Table 2 we present for each method the type of processor, its clock frequency and the programming environment used to write the code, the number of discretisation steps (modes for modal methods, waves for GT, and points for FDTD) in the transverse (x) direction, the number of discretisation steps (points or sections) in the longitudinal (z) direction, the computer memory (RAM) occupied by the programme, the total computing time required to calculate data shown in Fig. 4(c) with the spectral resolution of 2 nm (i.e., for 501 wavelengths), and the 'equivalent' time obtained by scaling the real computing time to the CPU clock frequency of 1 GHz.

Due to the various computer systems and platforms used by different laboratories a detailed comparison of the efficiency and accuracy of different methods has limited significance. It should be also realised that the algorithms were not fully optimised to minimise the numerical effort (CPU time and RAM memory). One can easily learn from Table 2 that memory requirements are low for all methods, including FDTD. The longer 'equivalent' computing time for the MoL compared to BEP1 and BEP2 is attributable to the application of Matlab, while all other methods use compiled codes. The shorter times of BEP1 and BEP2 against BEP3 document the advantage of the application of the FB (or analogous) formalism for periodic structures. It is not easy to compare the speed of GT and FDTD methods with others as they use rather different principles; they are nevertheless both well applicable for practical implementation.

5. Discussion and comments

All modelling methods have been shown to yield essentially equivalent results. It is thus time to give more detailed physical interpretation of the results and discuss their possible consequences on the behaviour of devices based on waveguide PCs.

Several general observations can be made from the spectral characteristics in Fig. 3. At the long-wavelength side of the band gap, the curves exhibit strongly oscillatory behaviour typical for low-loss regions. The oscillations are due to Fabry–Perot-type interferences in a grating of finite length. For shallow gratings, the resonances are less distinct due to lower reflection at the grating ends. The gratings with etching depths of 375 nm and more act as a nearly 100% low-loss reflector near the long-wavelength edge of the band gap. For shorter wavelengths, radiation (out-of-plane scattering) losses rise monotonously in the band gap and are never small at the short-wavelength side of the band gap. It has been found that the losses tend to remain moderate inside the band gap for gratings etched deeply (>125 nm) into the substrate. To better understand the grating behaviour, we also modelled the gratings with different ratios of the tooth/groove widths. The spectral position of the band gap is strongly dependent on the choice of these parameters, however. To keep the spectral position of the band gap unchanged at least in a rough approximation, we choose the following approach.

Neglecting the scattering into radiation modes, the Bragg wavelength of the waveguide grating with rectangular grooves is given by the expression

$$\lambda_B = 2(N_u L_u + N_e L_e), \tag{3}$$

where N_u, N_e and L_u, L_e are the effective indices of the (single) guided mode and the lengths of the unetched and etched sections of the grating (i.e., in the tooth and the groove), respectively. For the gratings described in the preceding section, the lengths were equal, $L_u = L_e = L_1 = 215$ nm. As long as the etched section supports a guided mode, we can choose, e.g., the tooth width L_u and calculate the groove width as

$$L_e = \left(\frac{\lambda_B}{2} - N_u L_u \right) \bigg/ N_e, \tag{4}$$

keeping the Bragg wavelength λ_B unchanged.

For deeply etched grooves, there is no guided mode in the groove. In this case, we suppose that the condition (3) is still valid for some 'equivalent index' N_e, which can be calculated from the condition (3) applied to the case of equal lengths, $L_u = L_e = L_1 = 215$ nm:

$$N_e = \frac{\lambda_B}{2L_1} - N_u. \tag{5}$$

We can then choose L_u and apply (4) to calculate L_e as before.

As is apparent from Fig. 4(c), the Bragg wavelength is difficult to determine for deeply etched gratings. We therefore chose the well-defined long-wavelength edge of the band gap, instead, namely, $\lambda_B = 1.418\,\mu m$. At this wavelength, the effective refractive index of the unetched guide is $N_u = 1.7812677$.

For brevity, we present here only the results for the deeply etched (750 nm) grating. Using Equations (4) and (5), we arrived at the following set of tooth/groove lengths L_u/L_e: 350/56, 300/115, 200/233, 100/350, and 50/409 nm. The results of modal reflectance and loss calculations for such gratings are shown in Fig. 5.
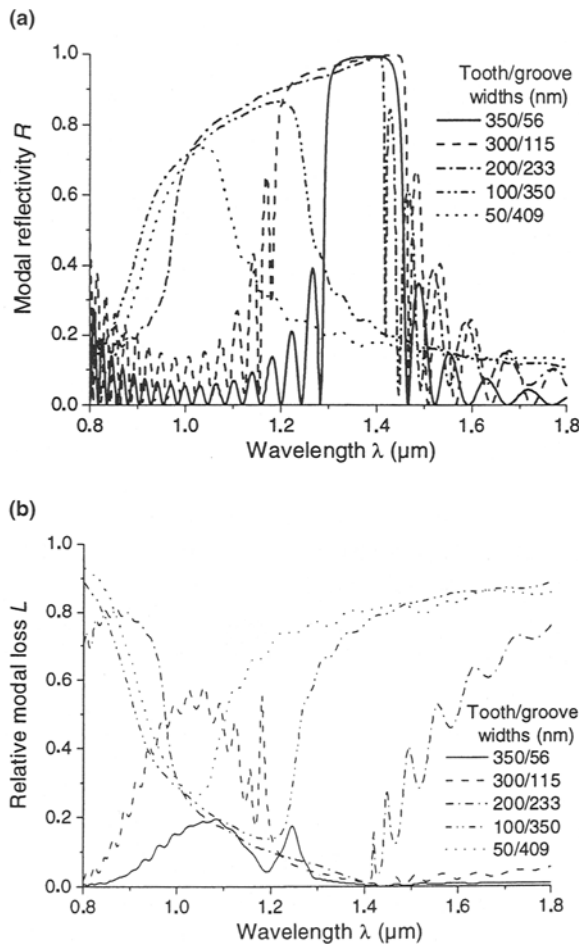
Fig. 5. Modal reflectance and losses of waveguide Bragg gratings with varying mark–space ratio. (a) Modal transmittance, (b) modal losses. Tooth/groove widths shown in the legends.

It can be concluded from both the reflectance and loss spectra in Fig. 5 that deep gratings of the 'notch' type (with comparatively wide teeth and narrow grooves) exhibit relatively low losses inside the band gap. This is in agreement with the prediction made in (Krauss and De La Rue 1996). However, another prediction made in (Krauss and De La Rue 1996), viz. that retaining some guiding layer inside the teeth (i.e., not etching completely through the wave-guide) should be beneficial for reducing loss, could not be confirmed, cf. Fig. 3(a), (b) (guiding retained) and Fig. 3(c) (no guiding retained).

Although the calculation of spectral characteristics of the waveguide grating yields its important 'integral' technical parameters like modal reflectance and transmittance, for better understanding of underlying physical effects, the modal characteristics of the grating itself are helpful. They can be calculated by the methods discussed in this paper, too. Denoting the phase shift of the mth FB mode in the grating (see section 'Modelling methods' above) by φ_m and the (total) period length by Λ, the corresponding wave number of the mth FB mode can be calculated as

$$k_m^{FB} = \varphi_m/\Lambda. \tag{6}$$

It is useful to define the effective refractive index $n_{\text{eff},m}^{FB}$ of the mth FB mode by the relation

$$k_m^{FB} = k_0 n_{\text{eff},m}^{FB} = \frac{2\pi}{\lambda} n_{\text{eff},m}^{FB}. \tag{7}$$

The application of efficient absorbing conditions makes it possible to calculate correctly the complex phase shift φ_m and correspondingly, the complex FB wave number (6), and the complex effective refractive index of the FB mode (7) in structures exhibiting out-of-plane radiation losses. In Fig. 6 we present results of such calculations of the lowest-order FB mode for two comparatively low-loss gratings, namely the shallow grating with the etching depth of 250 nm and the tooth/groove widths of 215/215 nm (i.e., with a period $\Lambda = 430$ nm), and the 750 nm deep etched grating with the tooth/groove widths of 350/56 nm ($\Lambda = 406$ nm).

The band diagram (photon frequency versus Re{k^{FB}}) of the shallower grating is shown in Fig. 7 in the form more commonly used for PBG structures. On the horizontal axis, the real part of the FB wave number is normalised with respect to a half of the grating vector $K = 2\pi/\Lambda$ – the limit of the first Brillouin zone of the 1D PC. Above the light line (given by the phase velocity of light in the substrate), the band structure of the real waveguide PC is continuous due to the continuous spectrum of radiation modes. The fundamental FB mode is denoted as 'non-leaky' in Figs. 6 and 7 in the vicinity and inside the band gap, where its wave number is either real
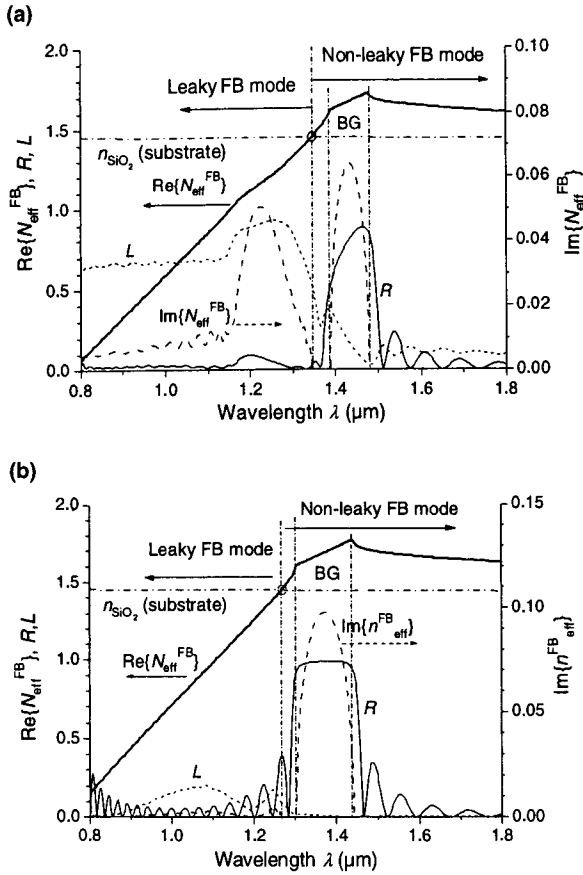
Fig. 6. Complex refractive index of the fundamental FB mode of the deeply etched waveguide grating; (a) Etching depth of 250 nm, tooth/groove widths 215/215 nm, period $\Lambda = 430$ nm, (b) etching depth 750 nm, tooth/groove widths of 350/56 nm, period $\Lambda = 406$ nm. BG denotes the band gap. Modal reflectance R and loss L are also shown (solid and short dash lines, respectively).

(outside the band gap) or imaginary (inside the band gap). We want to stress that this FB mode remains localised close to the guiding layer without any coupling to radiation modes.

From Figs. 6 and 7, the behaviour of the Bragg grating can be better understood. The spectral position of the band gap is accurately defined by the character of the wave number (or the effective refractive index) of the fundamental FB mode: as far as the fundamental FB mode is non-leaky, its wave number is real outside the band gap and purely imaginary inside the band gap. When the real part of the effective index of the fundamental FB mode is smaller than the refractive index of the substrate (for $\lambda < 1.35\,\mu$m in Fig. 6(a) and for $\lambda < 1.27\,\mu$m in Fig. 6(b), the FB mode becomes leaky and starts to radiate into the substrate. In terms of the 'classical' integrated optics, the Bragg grating now couples light into the substrate and acts as a grating coupler.
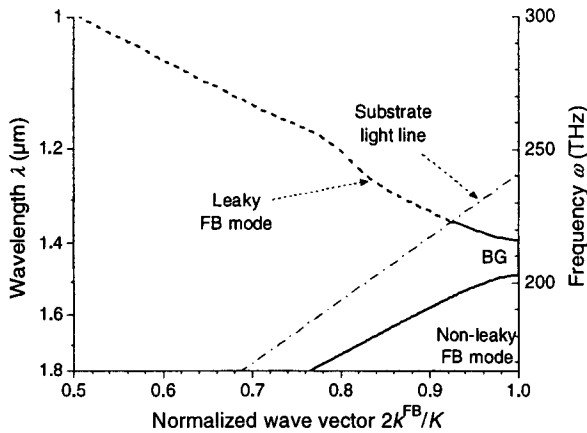
Fig. 7. Band diagram of the waveguide grating of Fig. 6(a) (etching depth 250 nm, tooth and groove widths 215 nm). BG denotes the band gap.

Two mechanisms are responsible for out-of-plane losses by diffraction or scattering in the substrate and in the air. If the fundamental FB mode is not leaky, the losses ($L = 1 - R - T$) originate only from a mode mismatch between the fundamental guided mode and the fundamental FB mode. As shown in (Palamaru and Lalanne 2001) where an accurate and analytical model for the losses is proposed and tested against electromagnetic theory, the losses in the band gap vary linearly with the square of the integral overlap between the fundamental guided and FB modes. For the two waveguide gratings considered in Fig. 6, this mode mismatch is responsible for the losses in the long-wavelength region and in the gap. In the short wavelength region, the situation is more complex. Losses originate from the mode mismatch and from the leakage of the fundamental FB. Moreover, for shorter wavelengths, higher-order leaky FB modes are substantially excited at the front and back grating interfaces, which contributes to increased loss.

Fig. 8 shows the comparison between the fundamental guided mode at $\lambda = 1.43$ (solid curve) and the fundamental FB modes computed at several wavelengths. For simplicity, we present here the graph for the shallower grating in which the lossless behaviour is more pronounced. For frequencies inside the band gap, it is understood that the integral overlap decreases with decreasing wavelengths. Correspondingly, the losses increase and the reflectance inside the band gap decreases. It is the reason why the loss reaches its minimum (very close to zero) on the long-wavelength side of the band gap. This mode mismatch is also responsible for the deformation of the reflectance spectral curves inside the gap, (cf. R and L curves in Fig. 6(a) and (b). The fact that the overlap integral decreases with decreasing wavelengths can be understood if we realise that light is more confined in the air gap for shorter wavelengths. Consequently, the FB mode 'sees' less material and the fun-
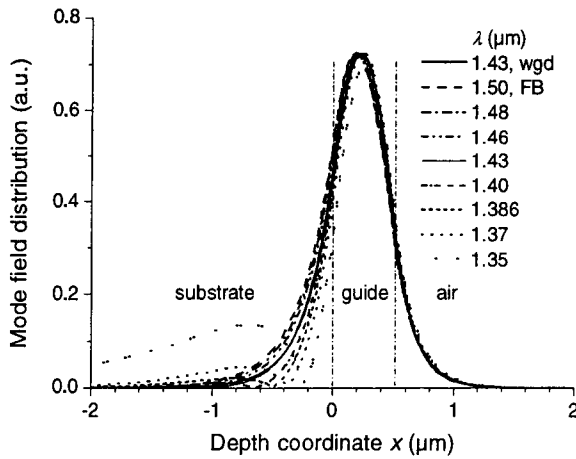
Fig. 8. Field distributions of the guided mode in the input waveguide and of the FB modes in the middle of the tooth of the waveguide grating of Fig. 6(a). Solid – waveguide mode at $\lambda = 1.43\,\mu m$ (i.e., at the centre of the band gap; the wavelength dependence of the mode field distribution is rather weak); other curves stand for the fundamental FB mode at the wavelengths indicated in the legend.

damental FB mode differs from the fundamental guided mode. This is also reflected in the real part of the refractive index of the FB mode that decreases inside the band gap as the wavelength decreases.

6. Conclusions

The spectral behaviour of a waveguide Bragg grating was modelled using five spectral methods and one FDTD method developed independently in different European laboratories. Very good mutual agreement indicates that all methods work well. It has been found that material dispersion of the SiO_2/Si_3N_4 system does not significantly affect the results. Light propagation in the waveguide grating was physically interpreted using the concept of FB eigenmodes of the grating as a 1D photonic crystal. The existence of a lossless FB mode in gratings with grooves etched deeply into the substrate was confirmed. Two basic sources of out-of-plane losses of the waveguide PC were identified, namely the coupling of FB modes in the waveguide grating to radiation modes (light 'outcoupling' by a periodic structure of the PC), and mismatch between field distributions of a FB mode in the grating and the eigenmode of the input waveguide.

Acknowledgements

References

Benisty, H., C. Weisbuch, D. Labilloy, M. Rattier, C.J.M. Smith, T.F. Krauss, R.M. De La Rue, R. Houdé, U. Oesterle, C. Jouanin and D. Cassagne. *J. Lightwave Technol.* **17** 2063, 1997.

Bérenger, J.-P. *J. Comp. Phys.* **114** 185, 1994.

Bienstman, P. and R. Baets. *Opt. Quant. Electron.* 31, 2001.

Bienstman, P., H. Derudder, R. Baets, F. Olyslager and D.D. Zutter. *IEEE Trans. Microwave Theory Tech.* MTT49, 2001.

Charlton, M.D.B., S.W. Roberts and G.J. Parker. *Mat. Sc. Eng. B* **49** 155, 1997.

Chew, W.C., J.M. Jin and E. Michelsen. *Microwave Opt. Technol. Lett.* **16** 363, 1999.

Čtyroký, J., S. Helfert and R. Pregla. *Opt. Quant. Electron.* **30** 343, 1998.

Guekos, G., ed., *Photonic Devices: How to Model and Measure, Pages, Photonic devices: How to Model and Measure.* Springer, Berlin, 1998.

Helfert, S.F. and R. Pregla. *J. Lightwave Technol.* **16** 1694, 1998.

Joannopoulos, J.D., R.D. Meade and J.N. Winn. *Photonics Crystals, Molding the Flow of Light.* Princeton, Princeton University Press, Pages, 1995.

Johnson, S.G., S. Fan, P.R. Villeneuve and J.D. Joannopoulos. *Phys. Rev. B* **60** 5751, 1999.

Krauss, T.F. and R.M. De La Rue. *Appl. Phys. Lett.* **68** 1613, 1996.

Mekis, A., J.C. Chen, I. Kurland, S. Fan, P.R. Vileneuve and J.D. Joannopoulos. *Phys. Rev. Lett.* **77** 3787, 1996.

Palamaru, M. and P. Lalanne. *Appl. Phys. Lett.* **78** 1466, 2001.

Pregla, R. *MoL-BPM Method of Lines Based Beam Propagation Method. Methods for Modeling and Simulation of Guided-Wave Optoelectronic Devices (PIER 11).* W.P. Huang. EMW Publishing, Cambridge, Massachusetts, USA, p. 51. 1995.

Pregla, R. *The Impedance/Admittance Transformation – an Efficient Concept for the Analysis of Optical Waveguide Structures.* Integrated Photonics Research, Santa Barbara, USA, OSA. 1999.

Rogge, U. and R. Pregla. *J. Lightwave Technol.* **11** 2015, 1993.

Scarmozzino, R., A. Gopinath, R. Pregla and S.F. Helfert. *IEEE J. Sel. Top. Quan. Electron.* **6** 150, 2000.

Silberstein, E., P. Lalanne and J.-P. Hugonin *J. Opt. Soc. Am.* (in press) 2001.

Stoffer, R., H.J.W.M. Hoekstra, R.M. de Ridder, E.v. Groesen and F.P.H.v. Beckum. *Opt. Quant. Electron.* **32** 947, 2000.

Sudbo, A.S. *Pure Appl. Opt.* **3** 381, 1994.

Sztefka, G. and H.-P. Nolting. *IEEE Photonics Technol. Lett.* **5** 554, 1993.

Taflove, A. *Computational Electrodynamics: The Finite-Difference Time–Domain Method*, Norwood, MA, Artech House Inc., Pages, 1995.

Yablonovich, E. *Phys. Rev. Lett.* **58** 2059, 1987.